Current Opinion in Colloid & Interface Science 20 (2015) 272–281

Contents lists available at ScienceDirect

Current Opinion in Colloid & Interface Science

journal homepage: www.elsevier.com/locate/cocis

Particle shape effects in colloidal crystals and colloidal liquid crystals: Small-angle X-ray scattering studies with microradian resolution

Andrei V. Petukhov *, Janne-Mieke Meijer, Gert Jan Vroege

van 't Hoff laboratory for Physical and Colloid Chemistry, Debye Institute for Nanomaterials Science, Utrecht University, Padualaan 8, 3508 TB Utrecht, The Netherlands

ARTICLE INFO

Article history:
Received 5 July 2015
Received in revised form 27 September 2015
Accepted 28 September 2015
Available online 9 October 2015

Keywords:
Colloidal crystal
Colloidal liquid crystal
Small-angle X-ray
Scattering
Microradian resolution
Anisotropic colloids

ABSTRACT

Small-angle X-ray scattering (SAXS) is an indispensable tool in structural investigations of self-assembled colloidal crystals and colloidal liquid crystals. This paper reviews recent studies of the particle shape effects on the crystal structure as revealed by SAXS. Rod-like, plate-like, biaxial board-like as well as cubic-like shapes are discussed. Since relatively large, (sub)micron particles are often used in these studies, we describe the principles of the microradian X-ray diffraction technique that allows detailed characterisation of the periodic order including the determination of the intrinsic width of the Bragg peaks.

1. Introduction

Structures on the mesoscales, ranging from about a nanometre to a micron, play a key role in a broad range of research fields such as soft matter [1,2], heterogeneous catalysis [3] and biology [4,5]. They can be studied either in direct-space using microscopy or in reciprocal-space using scattering that are complementary to each other.

Microscopy data is more straightforward and can usually be interpreted in an easier way. However, it yields information on small sample volumes the choice of which is often biased by the observer. Electron microscopy is very powerful as it can access all scales of interest down to the atomic scale. However, this technique is limited in accessing bulk structures and is not suitable for in-situ and time-resolved studies. The latter can be solved using optical microscopy but only on large scales. Recent developments of super-resolution optical microscopy techniques [6] are a great step forward but they are applicable only to systems that can be labelled with fluorescent dyes.

In contrast, scattering techniques are able to provide mesoscopic structural data averaged over macroscopic volumes. They are often perfectly suitable for in-situ and time-resolved studies in the bulk. Light scattering is easily affordable but only provides access to a very limited range of q-values and often suffers from multiple scattering. Small-angle neutron scattering (SANS) has a number of important advantages such as contrast variation possibilities and sensitivity to magnetic structures. However, low brightness of neutron sources limits the range of applications of SANS. Nowadays small-angle X-ray scattering (SAXS) is widely recognised as an indispensable structure characterisation tool at the mesoscopic scales. Recent developments of synchrotron sources and X-ray detectors provide a very fast and effective tool to study colloidal crystals and their real-time development. The high penetration power of X-rays makes SAXS applicable to almost all system types. In addition, the intrinsically low contrast of all materials for X-rays ensures, in the vast majority of cases, a high quality of the scattering data that is free of multiple scattering contributions. SAXS also gives access to a broad range of spatial scales from a nanometre to microns. Moreover, as we shall discuss in more detail below, positional correlations on distances up to submillimetre can be accessed from the width of diffraction peaks measured with microradian resolution.

In this review we shall focus our attention onto the recent studies of crystals and liquid crystals obtained by the self-assembly of colloidal particles. Their self-assembly can be directed in various ways, for instance by applying an external electric or magnetic field [7,8]. Alternatively, one can vary the particle shape to achieve novel colloidal lattices [9–11]. The use of strongly anisotropic shapes leads to a very rich phase behaviour including numerous liquid-crystalline states, which are of interest for researchers and engineers to prepare new nanomaterials with novel symmetries using self-assembly techniques. Their crystal structures, however, have to be carefully characterised in order to be employed as such and this is where SAXS analysis plays an important role.

The rest of this review is organised as follows. Section 2 is devoted to the discussion of how to achieve microradian resolution in SAXS

* Corresponding author. Tel.: +31 30 253 1167; fax: +31 30 253 3870.
E-mail address: a.v.petukhov@uu.nl (A.V. Petukhov).
URL: http://www.uu.nl/staff/APetoukhov/ (A.V. Petukhov).

http://dx.doi.org/10.1016/j.cocis.2015.09.003
1359-0294/

experiments. Section 3 provides a short summary of the form factor scattering that can be measured in dilute suspensions. This is followed by an overview of the recent developments in the studies of liquid crystals formed by rod-like, plate-like and board-like colloids in Section 4. In this part the behaviour of these anisotropic particles in external magnetic fields is also reviewed. In Section 5, we describe the investigations of structures formed by cubic-like colloids which have been performed in the last few years. Finally, a short summary is given in Section 6.

2. Microradian X-ray diffraction

Application of X-ray scattering to study the self-assembly of large, (sub)micron-sized colloids is challenging due to the enormous, 3 to 4 orders of magnitude, difference between the scale of interest and the X-ray wavelength λ that results in very small diffraction angles, $2\theta \sim \lambda/d \sim 1 \ldots 0.1$ mrad, where d is the period of the structure. To resolve such diffraction patterns, one needs to have a resolution significantly better than these values of 2θ. Moreover, very useful information is contained in the width of the diffraction peaks, which sets the resolution demands much higher.

For example, in a perfect but small crystal the peak width is determined by the inverse crystal size. This finite-size broadening is the same for all diffraction peaks but can depend on the direction in 3D reciprocal space for crystals with anisotropic shape. The broadening is the strongest in the direction of the smallest crystal size (e.g., along the normal for a thin crystalline film). Moreover, diffraction peaks can be broadened by defects and strain fields, which deform the ideal crystal lattice. This "second-type disorder" in the terminology of Guinier [12] leads to peak broadening that depends on the q-value. Since in small-angle X-ray scattering experiments multiple diffraction orders can often be simultaneously measured, it is straightforward to apply the Willamson–Hall analysis to colloidal crystals [13], which allows one to determine the typical crystal size and the strength of the strain field.

To illustrate what type of information can be revealed by SAXS, we show in Fig. 1 two examples of 2D patterns measured with microradian resolution using different crystals of colloidal spheres [14,15]. There are strong similarities between the patterns and the data may have looked nearly identical if measured with a lower resolution. However, thanks to the microradian resolution, one can now see a striking difference in the width of the reflections. In Fig. 1a one can also see that the peak broadening can be anisotropic. The width δq_r in the radial direction is the measure of the spatial extent of the periodic order and the strain. The width of the peak δq_ϕ in the orthogonal azimuthal direction can possess additional contributions originating from fluctuations of the exact orientation of the crystallographic axes within the irradiated area of the sample. In the latter case the reflections often possess an arc-like shape. Moreover, crystal imperfections can lead to additional scattering in between the Bragg peaks, which can also bring useful structural information on the colloidal structures.

To summarise, small-angle X-ray diffraction is able to provide a wealth of information about the periodic order and imperfections in colloidal crystals, just similar to X-ray diffraction (XRD) in ordinary, atomic or molecular, crystals. To obtain this information is, however, challenging, especially for crystals made of large (sub)micron particles. Ideally, one would need to achieve resolution in reciprocal space corresponding to submillimetre direct-space distances to be able to probe positional correlations on a distance of the order of hundred lattice periods. For X-rays with the wavelength of $\lambda \sim 0.1$ nm, the angular resolution of the order of a microradian is therefore required.

How can one actually achieve the microradian resolution in small-angle X-ray scattering experiments? Does one need to build a very long beamline with extremely large sample-detector distance as in Ref. [16]? Does one need to use a "pencil-beam", *i.e.* a very thin X-ray beam? Or, does one need instead to strive for achieving a very parallel beam? To correctly answer these questions, we need to recall that X-ray scattering is essentially a coherent process. To be able to achieve a reciprocal-space resolution of δq, one has to make sure that waves scattered at points separated by a distance of the order of $2\pi/\delta q$ are still able to interfere at the detector. It is therefore important to consider the beam coherence.

2.1. Transverse coherence and angular resolution

Transverse coherence is related to the finite size of the X-ray source, the electron beam in the synchrotron in our case. Random summation of waves emitted at different points of the incoherent source leads to random modulation of the phase of the X-ray wave in the transverse direction [17]. The transverse coherence length l_{tr} is defined as the distance along a wave front over which the phase fluctuations become significant. As a result, the interference of waves scattered by particles separated by more than l_{tr} vanishes after averaging over all random realisations. For a freely propagating X-ray wave the transverse coherence length $l_{tr} = L\lambda/(2d)$ [17] is determined by the source-sample distance L, the X-ray wavelength λ and the transverse source size d. By using typical values of $L \sim 50$ m, $\lambda \sim 0.1$ nm and $d \sim 0.1 \ldots 1$ mm, one can estimate $l_{tr} \sim 2.5 \ldots 25$ μm. This means that the existing synchrotron sources have the potential of probing positional correlations on distances up to a few microns or even tens of microns. With the current upgrade plans of the modern synchrotrons such as the ESRF [18], even submillimetre values of l_{tr} can become feasible.

Fig. 2 shows a few illustrations of the possible SAXS setup schemes that can be used. Double-headed vertical arrows denote refractive

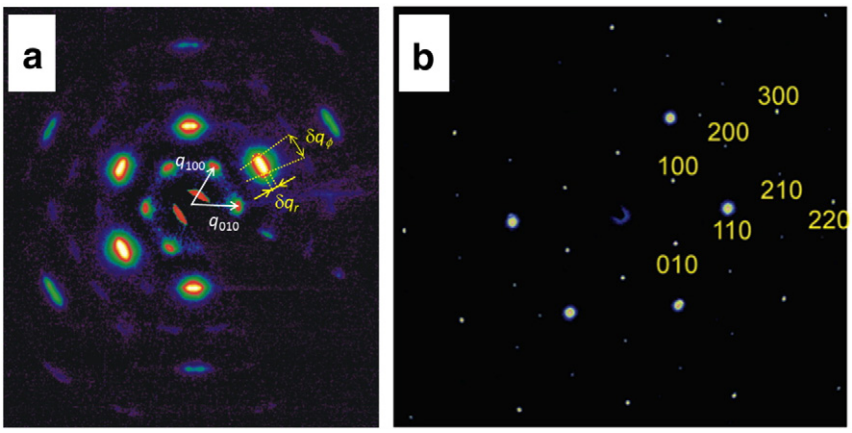

Fig. 1. Examples of the small-angle diffraction patterns measured with an angular resolution better than 10 μrad. The pattern in (a) is measured from a colloidal crystal of 425 nm polystyrene microspheres grown on a glass substrate using the vertical deposition technique [14]. The pattern in (b) is obtained from a sedimentary crystal of 224 nm silica spheres [15]. The intense diffraction peaks of the 110 family in panel (b) strongly saturate the detector and their apparent width is exaggerated.

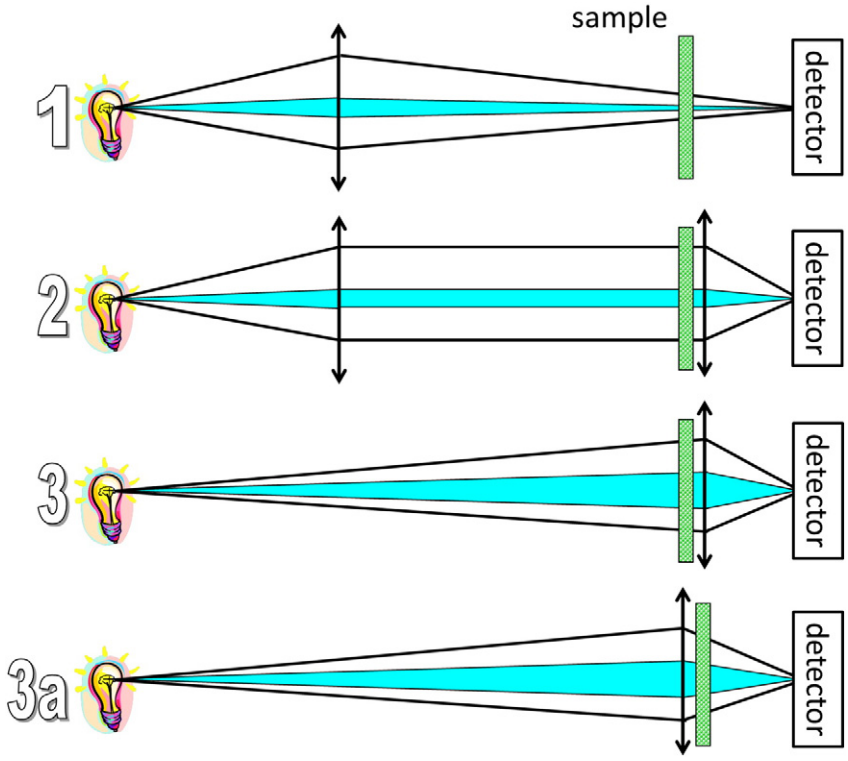

Fig. 2. Various possible concepts of small-angle X-ray scattering setup using focussing optics as discussed in the text. The "lamp" stands for the partially coherent source of X-rays. Optical elements such as the monochromator are not shown. It is assumed that the monochromator does not disturb nor focus the beam. The shaded area denotes a coherent patch, the size of which is exaggerated for better visibility.

and/or reflective optical elements that can focus the beam. These optical elements can be placed at different locations at the beamline, such as at a significant distance from the sample in the optics hutch, or in a close vicinity of the sample in the experimental hutch. Scheme 1 can be seen as a realisation of the "pencil-beam" concept, where the focussing element is placed far before the sample. Scheme 2 utilises a focussing element to create a parallel beam that passes through the sample and is then focussed on the detector. While, in Schemes 3 and 3a the beam is freely propagating to the sample and focused on the detector in the vicinity of the sample. The difference between Schemes 3 and 3a is that the positions of the focussing element and the sample are exchanged.

As illustrated in Fig. 2 by shading, focussing the beam before it hits the sample can increase the beam intensity and reduce the spot size. However, it will also reduce the transverse coherence length l_{tr} at the sample position. This can be seen as an increase of apparent source size d, as viewed from the sample position through the focussing element. Scheme 1 might be advantageous if one needs to perform spatially-resolved measurements but it is obviously the worst for achieving the highest angular resolution because the transverse coherence length is too short at the sample position. Scheme 2 and, especially, Scheme 3 yield much longer l_{tr} in the sample. Scheme 3 is the main concept of the microradian X-ray diffraction setup, which exploits compound refractive lenses [19••]. This setup [7,20••] has been routinely used by the authors to study colloidal crystals at the Dutch-Belgian beamline DUBBLE [21] at the European Synchrotron ESRF (Grenoble, France). However, in practice the positions of the focussing lens and the sample are exchanged (Scheme 3a) due to the practical realisation that the relatively small aperture of the lens can restrict measurements at larger scattering angles. In this setup the beam hitting the sample is converging but, due to the small distance between the lens and the sample, the reduction of the transverse coherence length in the beam due to focussing is yet negligible. In addition, in Scheme 3 a part of the scattered photons are absorbed in the lens so that one needs a larger radiation dose at the sample to measure the same scattered intensity as in Scheme 3a.

2.2. Longitudinal coherence and rocking curve measurements

The final spectral width $\Delta\lambda$ of the X-ray wave after a monochromator leads to a finite coherence in the beam in the longitudinal direction, i.e. along the beam. As the result of random summation of different spectral components, the wave can be seen as a sequence of wave packets of a length of the order of $l_{\mathrm{long}} = \lambda^2/(2\Delta\lambda)$, which are not coherent with each other [17]. For typical values at a synchrotron beamline, $\lambda \sim 0.1$ nm and $\Delta\lambda/\lambda \sim 10^{-3} \ldots 10^{-4}$, one gets $l_{\mathrm{long}} \sim 0.05 \ldots 0.5$ μm. This value may seem to be too small if one aims to characterise structures with a period up to micron(s).

Let us consider two colloidal particles separated by a certain distance l in the longitudinal direction. A given wave packet will not reach the particles simultaneously because of the difference of l in the distance from the source. However, most of this pathlength difference l is compensated by the difference in the pathlength, $l(1 - \sin^2 2\theta)$, the scattered waves have to travel to the detector. Detailed analysis of the problem [22•,23] reveals that in the longitudinal direction the conditions for coherent interaction between the waves is almost always fulfilled and the finite monochromaticity can be usually neglected in the conditions of a small-angle scattering experiment.

This fact can be used to determine the width of the diffraction peaks in the longitudinal direction with a very high resolution for a single colloidal crystal in the so-called rocking curve measurement. Here one records the intensity of a certain diffraction peak as a function of the orientation of the single crystal. With this measurement one can detect peak broadening as small as one millionth of the wavevector of the incident wave [22•]. Note that the rocking curve measurement is only able to probe the peak width along the beam, i.e. in the direction normal to the Bragg wavevector.

As a final remark, let us return to our choices of the possible measurement schemes, Fig. 2. In the usual realisation of the microradian X-ray diffraction setup (Scheme 3a) the incident beam is converging at the sample position and thus contains plane-wave components with slightly different directions. This might result in a reduction of the resolution in the rocking curve measurements. For the latter geometries offering more parallel beam (Schemes 2 and 3) are preferred.

3. Dilute dispersions and form factor

We remind the reader that in principle information about the size and the shape of individual colloidal particles can be obtained from scattering experiments using dilute suspensions. The resulting scattering pattern can be described using the form factor, which is usually defined as the square of the total scattering amplitude normalised to 1 at small q. For example, for a cuboid shape with a uniform density and size L_i along i th direction the form factor is given by [12]

$$P\left(\vec{q}\right) = \left(\frac{\sin(q_x L_x/2)}{q_x L_x/2}\frac{\sin\left(q_y L_y/2\right)}{q_y L_y/2}\frac{\sin(q_z L_z/2)}{q_z L_z/2}\right)^2, \quad (1)$$

which remains close to 1 as long as $q_i \ll 2\pi/L_i$ and decays at larger q displaying characteristic fringes. Simply stated, this means that the intensity will have a faster decay along q when L_i becomes larger. For example, for rod-like particles with a strongly anisotropic shape, $L_x \gg L_y$ & L_z, the scattering intensity will extend to much larger q-values in the y,z-plane in comparison to the x-direction. Qualitatively, the form factor of a single rod looks therefore like a plate in reciprocal space and vice versa. Of course, the form factor can in practice only be measured on dilute dispersions when the positions of the particles are not correlated. Unless an external field is applied, this implies that also the orientations of the particles are not correlated and the scattering pattern of the individual particles is orientationally averaged. Averaging their form factors in reciprocal space leads to the characteristic decay of scattering intensity for rods and plates with high aspect ratio within the intermediate q-regime:

$$\begin{matrix} P(q) \propto q^{-1}\ (\text{rods}) \\ P(q) \propto q^{-2}\ (\text{plates}) \end{matrix} \left(2\pi/L_{\text{largest}} \ll q \ll 2\pi/L_{\text{smallest}}\right). \quad (2)$$

On the other hand, the orientational averaging obviously also obscures specific features of the form factor, e.g. making it hard to distinguish the scattering patterns of cubic particles and polydisperse spherical particles.

The particle form factor also plays an important role in the small-angle X-ray diffraction from colloidal crystals and liquid crystals. The visibility of a specific Bragg peak can be low if it appears close to a form factor minimum (e.g., the peaks of the 300 family are hardly visible in Fig. 1). The position of a relatively broad Bragg peak can be shifted by the q-dependence of the form factor. One has to take into account those effects in the analysis of the experimental data.

4. Colloidal liquid crystals

The colloidal counterparts of liquid crystals have been known and studied since 1925 when Zocher reported [24] spontaneous ordering in dispersions of vanadium pentoxide and iron (hydr)oxide particles. Above a certain volume fraction a randomly oriented isotropic dispersion of vanadium pentoxide first formed spindle-shaped droplets and on standing a layer with typical birefringent optical defects which betrayed nematic liquid-crystalline order (orientation along a single axis). In the bottom part of his 15–30 year old iron (hydr-)oxide suspensions he observed iridescence – which reformed after shaking – and deduced that the colloidal particles spontaneously stacked into layers, ascribing the bright colours to Bragg reflection of visible light on the layers typical of a smectic liquid crystal. It later turned out that he was completely right in his interpretation although the particle shapes he assumed were wrong without direct means to establish these at the time. More details about the historical developments can be found in a recent review paper by Lekkerkerker and one of us [25]. In contrast to common (low-molecular weight) liquid crystals X-ray diffraction was originally not available at the small angles required so that optical Bragg reflection, the study of textures and later direct imaging techniques were used to study their colloidal analogues. In this review we will mainly discuss papers where small angle scattering or diffraction played an important role.

4.1. Rod-like particles

Although nematic phases in rod-like systems have been observed quite long ago, they were not much studied by SAXS for a long time, displaying relatively featureless scattering patterns. The full orientational distribution function and the nematic (orientational) order parameter S was determined from the analysis of the angular spread of X-ray diffraction patterns of Tobacco Mosaic Virus [26]. A combination of SAXS and wide-angle X-ray diffraction proved similar nematic ordering in a solution of more than 10 times smaller crystalline CdSe nanorods [27]. SAXS was used in combination with static light scattering [28] to characterise sterically stabilised particles of a natural sepiolite clay system confirming the q^{-1} dependence for rods, see Eq. (2). In rutile (TiO_2) nanorods with anisotropic photocatalytic properties SAXS also gave an estimate of the average lateral distance between the rods [29].

Liquid crystals with partial positional order were not so often studied by SAXS for rod-like colloid particles. A beautiful example of the complementary power of experiments in reciprocal and real space is a systematic study [30••] of μm-long rod-like silica particles with aspect ratios ranging from 3.7 to 8. Smectic-A ordering (1-D stacking of 2-D liquid-like layers) was found for L/D > 4.1 joined by a nematic phase above L/D > 5.0 in rough accordance with computer simulations on hard spherocylinders (see Fig. 3). At higher volume fractions further down in the sedimented samples, the rods did not form the expected fully crystalline phase but stacked into hexagonally ordered, non-correlated layers (smectic-B), probably due to polydispersity and/or charge. The SAXS measurements were instrumental in locating nematic regions which otherwise might have remained undetected.

4.2. Plate-like particles

Apart from clays [31], one of the first plate-like colloids showing discotic liquid crystals was hexagonal nickel II hydroxide $Ni(OH)_2$. SANS indicated 2-D hexagonal lateral ordering of the platelets but SAXS was needed to rule out the possibility of a smectic-B like layered structure and conclusively proved the existence of a columnar LC with 1-D liquid-like columns [32•]. The platelets were sterically stabilised by a polyelectrolyte and their effective aspect ratio was further varied by regulating the salt strength although not sufficiently to expect the nematic phase predicted by computer simulations [33]. The cubatic LC phase, consisting of a packing of small stacks of disks with cubic orientational order, predicted by the same computer simulations [33], is only locally ordered and would not easily be distinguished from the isotropic phase by scattering techniques; indications of its existence were only found by cryo-TEM much later [34]. The aspect ratio of hexagonal gibbsite ($Al(OH)_3$) platelets is larger due to their larger diameter and this was the first system to exhibit both nematic and (hexagonal) columnar LC phases [35•]. In this case the platelets were sterically stabilised by a polymer layer and dispersed in toluene to screen long-range interactions. Both this system and its aqueous version (usually stabilised by absorbed Al_{13} Keggin ions) were extensively studied by Lekkerkerker and co-workers.

An example of SAXS data is shown in Fig. 4. Due to the gravity-induced gradient of the osmotic pressure, co-existence of isotropic,

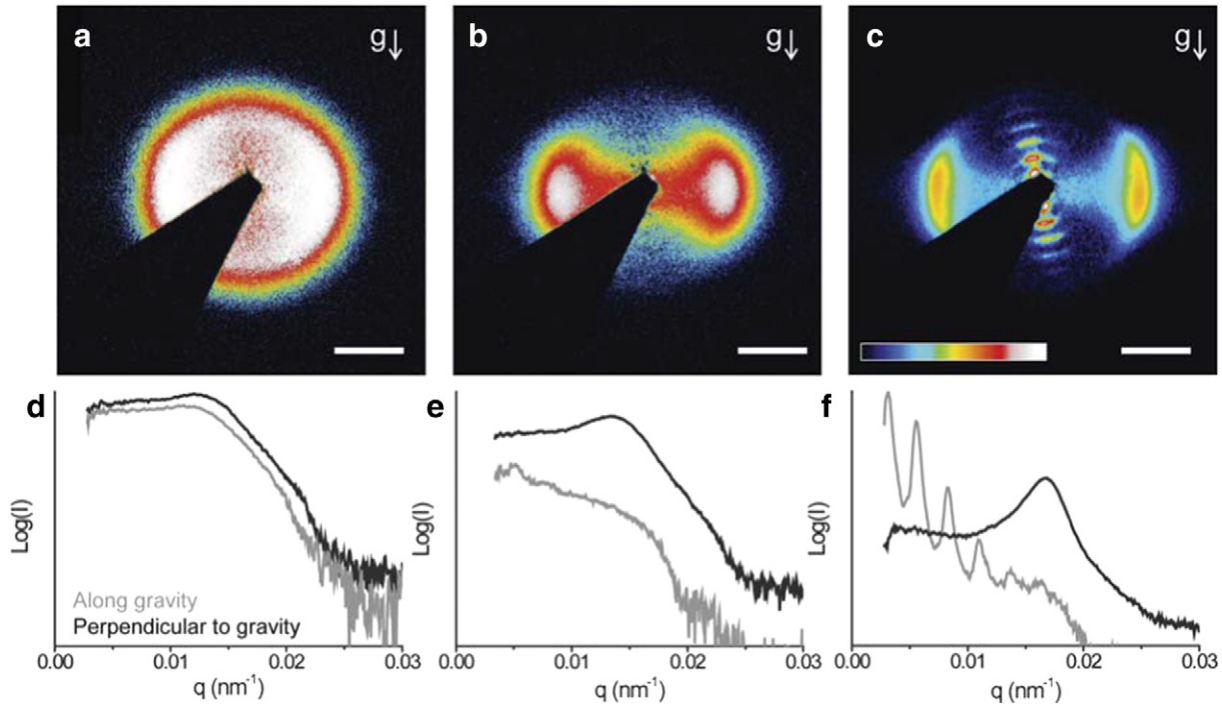

Fig. 3. SAXS patterns from a sediment of silica rods with length $L = 1.9$ μm and diameter $D = 235$ nm. Scattering patterns of the isotropic phase on top of the sediment (a), nematic (b) and smectic (c) liquid-crystalline phases below. White scale bars in (a–c) indicate 0.01 nm^{-1}. The intensity is given on the logarithmic scale using the false colour encoding given in (c). Panels (d–f) give the intensity profiles of the patterns shown in (a–c) in the horizontal (black) and vertical (grey) direction. Reproduced from Ref. [30••].

nematic and columnar phases can be clearly seen in a single capillary with a dispersion of sterically-stabilised platelets. Very careful analysis of the high-resolution SAXS patterns in the bottom part of the sediment [36•] was able to distinguish between a multidomain hexagonal columnar LC region with sharp reflections and a single-domain hexatic columnar LC region with short-range positional and long-range orientational order. Both phases coexisted within this sedimented sample where the hexatic region seemed to be caused by the need of the system to accommodate polydisperse disks at higher compression. Another way gibbsite platelets dealt with polydispersity on a long timescale was demixing into different domains with different intercolumnar spacings [37].

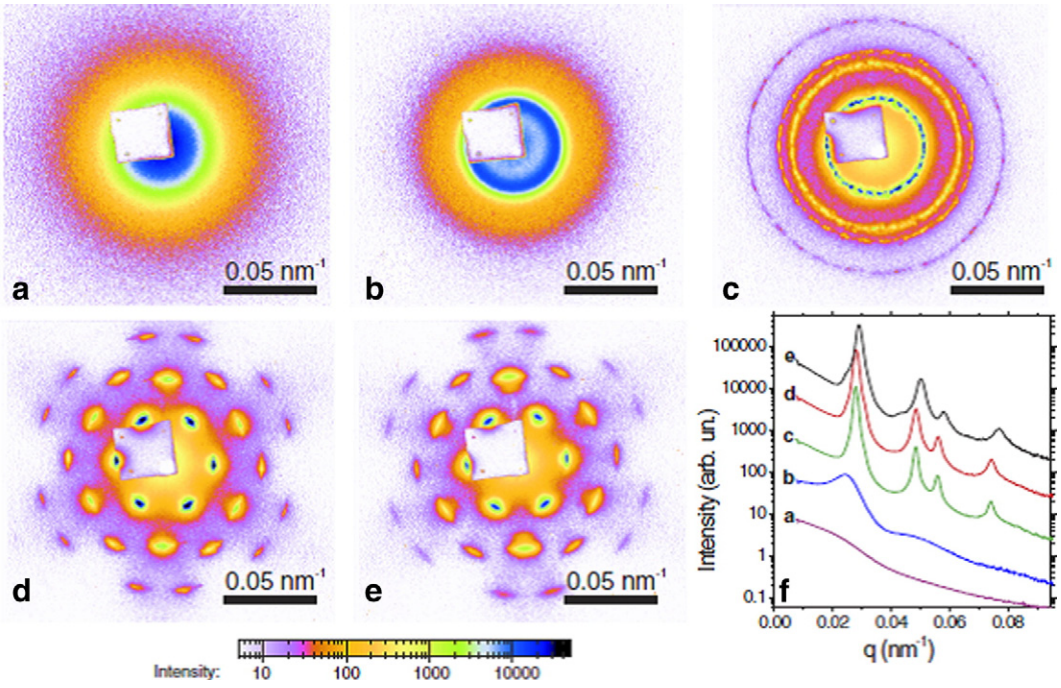

Fig. 4. SAXS patterns of the different phases observed in a suspension of sterically stabilised gibbsite platelets with diameter of 237 nm and polydispersity of 20%. From top to bottom in the capillary the isotropic (panel a), nematic (X-ray beam parallel to the director, panel b), multidomain hexagonal columnar (panel c) and single domain columnar phase with hexatic structure (panels d and e). A square-shaped lead beamstop was used to absorb the direct beam. Panel (f) shows the averaged radial profiles of the scattered intensity of the patterns shown in (a)–(e). Reproduced from Ref. [36•].

Positively charged aqueous gibbsite particles showed sol–gel behaviour (similar to clays) as they entered kinetically arrested states at both high and low salt concentrations. At intermediate salt concentrations, stable colloidal dispersions were formed up to relatively high concentrations, displaying a sequence of isotropic-nematic-columnar phases [38]. Interestingly, SAXS experiments revealed that the nematic phases at high salt concentrations or low platelet concentrations are of the usual (discotic) nematic type, while those at low salt/high platelet concentrations are of the columnar nematic (N_C) type, where increased lateral correlations indicate the formation of stacks of platelets. Kleshchanok et al. [39] dispersed charged gibbsite platelets in dimethyl sulfoxide (DMSO), a polar aprotic solvent leading to a long range of the electrostatic Coulomb repulsion between platelets, and did report a smectic-B, a layered liquid-crystalline phase consisting of hexagonally ordered particles (without inter-layer correlations).

Exfoliated inorganic nanosheets combine nanometre-size thickness with much larger lateral dimensions. Due to the huge difference in length scales they may display (lamellar) liquid-crystalline behaviour at very low concentrations as indicated by many higher-order SAXS peaks of the layered phosphate $K_3Sb_3P_2O_{14}$ [40]. This class of systems has already been extensively reviewed [41,42•], so we will not go into them here. Many natural clays also fall under this category although they tend to aggregate or gelate under many circumstances. Interestingly, since the first fleeting observation of LC behaviour in clays by Langmuir in 1938, a true isotropic-nematic phase equilibrium was only found in 2006 for lath-like nontronite [43••,44].

4.3. Board- or lath-like particles

In the previous section we just mentioned the clay nontronite consisting of lath-like particles with 3 different dimensions. The first mineral liquid crystal observed by Zocher [24] in fact turned out to consist of particles of similar shape. As extensively reviewed by Davidson [45] vanadium pentoxide consists of very long, 1 nm thin, semiflexible ribbons. At low volume fraction, these ribbons display an isotropic–nematic coexistence gap, which initially form a true nematic phase extending into a nematic gel beyond 1.5% volume fraction. Aligning particles by a shear field showed a cylindrically symmetric (uniaxial) alignment up to 4% volume fraction, above which SAXS suddenly displayed patterns with broken cylindrical (biaxial nematic) symmetry remaining for hours after the shear flow was stopped. This could be an indication of an underlying biaxial nematic LC phase, but could also be explained as a shear-induced gel state.

Another extensively studied system of board-like particles is the mineral goethite (α-FeOOH) grown under basic conditions [46]. Davidson and co-workers (see Ref. [47••] for a review) established that it consists of "rafts" of ordered crystallites of colloidal size with different crystallographic axes and properties in three perpendicular directions. The elongated form of these particles in one direction leads to liquid crystalline phases reminiscent of rods: nematic, smectic and columnar. The formation of the columnar phase is related to the high (length) polydispersity, so that particles form columns which order into a 2-D lattice [48,49]. However, on timescales at which Brownian motion allows fractionation smectic-A phases are split off even at polydispersities as high as 55% [50•]. At lower polydispersities the smectic-A is the most stable high-concentration phase [51] with often a very pronounced layer-like structure. By varying the synthesis conditions the size and aspect ratios of the goethite boards can be tuned [52] resulting in the observation of the first truly biaxial LC phases for colloidal systems [53•,54]. In the biaxial nematic phase the three different particle axes order in separate directions and liquid-like reflections are observed at different q in three perpendicular directions, of which one transforms into Bragg peaks for the biaxial smectic-A phase (see Fig. 5). Biaxial LC phases have formed a much studied and contested topic for more than 40 years (see Ref. [55] for an extensive overview and Ref. [56] for colloidal systems in particular).

4.4. External fields

The relatively large particle size in combination with pronounced and usually anisotropic material properties of mineral colloids leads to interesting coupling of LC behaviour to external fields (electric, magnetic, gravity, confinement, shear etc.; for a review see Ref. [57]) which can be followed by SAXS. Here we restrict ourselves to magnetic fields where a whole range of magnetic responses has been observed. Platelike gibbsite is *diamagnetic* and has a preference to align its short axis perpendicular to a magnetic field. In combination with a preferred direction of the short axis along the nematic director and the tendency to anchor the particles flat onto the surface this leads not only to an interesting response to a magnetic field [58] but also affects the location of the isotropic-nematic phase transition. A stronger response is found for $GdPO_4$ nanorods which are *paramagnetic* [59]. For *anti-ferromagnetic* goethite Davidson and co-workers [47••] found that the anti-parallel spin lattices do not compensate completely on the colloidal scale which results in a small permanent magnetic moment along the longest axis, whereas the easy axis of magnetization is along the shortest axis. Therefore, the permanent and induced magnetic moments compete leading to reorientation of the individual particles above a critical magnetic field. In LC phases this couples to the orientational and partial positional order, which for instance leads to the reorientation of the nematic phase by 90° and promotes the formation of a columnar from a nematic LC phase [48]. A new type of nematic–nematic phase separation into domains with particle director oriented either perpendicular or parallel to the applied field was also found, due to the fact that larger particles in a polydisperse sample start to reorient at a weaker magnetic field causing packing problems so that they spontaneously separate into a different phase [60]. Polydispersity also plays a role in the smectic phase [61] transforming to a columnar phase at high polydispersity and an intermediate smectic-C-like zig-zag structure at low polydispersity. The stability of the biaxial nematic is also affected by an external magnetic field in a subtle way [62]. Very recently, *ferromagnetic* platelets also have been studied. Martelj et al. [63] dispersed scandium-doped barium hexaferrite single-crystal nanoplatelets in a low-molecular-weight LC and created the first truly ferromagnetic liquid.

5. Cubic particle dispersions and crystals

The recent availability of colloids with a cubic shape has inspired investigations into their close-packed structures. A number of cubic-like shapes have been studied, such as near perfect cubes [64••,65], cubes with rounded edges [66,67•] or truncated edges [68–70], and even convex or concave faces [65]. The increased research efforts stem from the fact that a cubic shape allows the assembly of structures with much higher packing fractions than conventional spheres and in addition increases the interparticle contact. Therefore, these structures are of interest for both fundamental studies and new functional nanomaterials.

Here we discuss those studies that have employed SAXS for clarifying the structures assembled by cubic-like particles. SAXS is more equipped for the structural investigations because the cubic particles are typically made of metal-based materials, such as palladium [64••], gold [65], lead selenite [69], and iron (hematite and magnetite) [67•,68,71]. Despite the power of SAXS measurement the structural investigations are often combined with electron microscopy or other direct space imaging techniques because it remains difficult to determine the exact orientation of the cubic particles on the crystal lattice from the SAXS patterns alone.

Two distinct size ranges of cubic colloids have been explored to date, which we note because this changes certain aspects of the assembly studies. The first size range is the cubic particles between 1–100 nm that are typically monocrystalline and stabilised by a ligand shell. We will refer to these as *cubic nanoparticles*. The second size range is that between 100–1500 nm, which we will refer to as the *cubic*

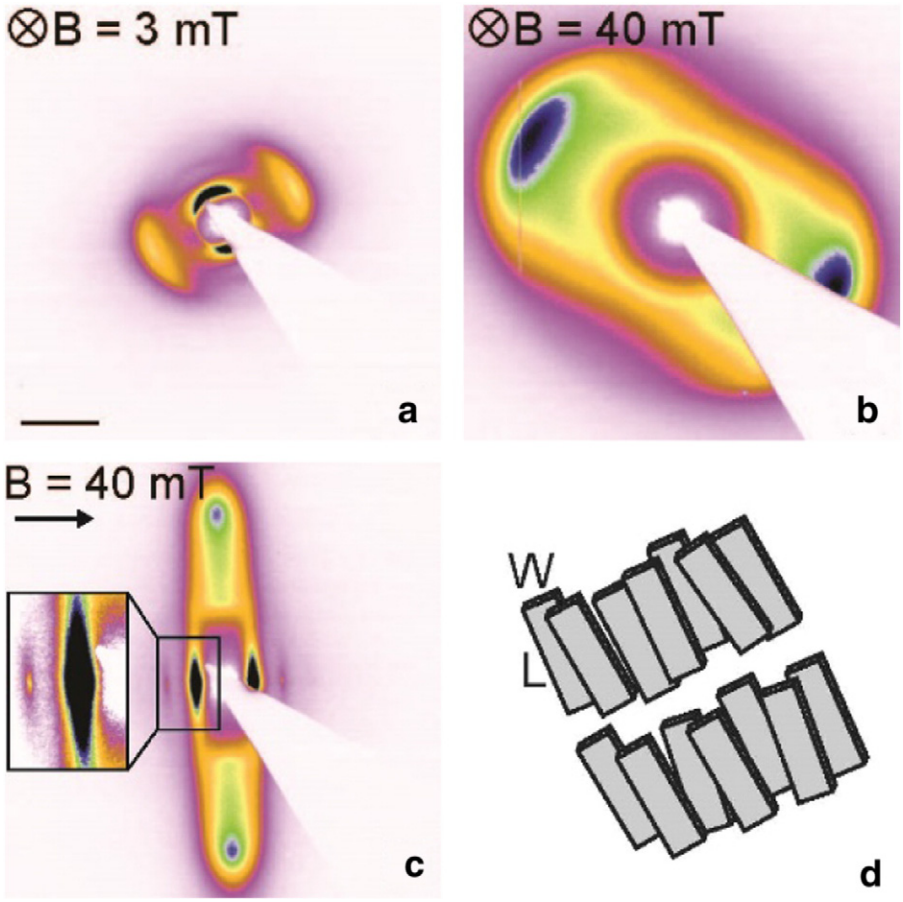

Fig. 5. SAXS patterns of the biaxial smectic-A phase in a capillary. To align the domains, a small magnetic field of (a) 3 mT and (b) 40 mT parallel to the X-ray beam, and of (c) 40 mT perpendicular to the X-ray beam (including zoom) was applied. The black scale bar in (a) is 0.05 nm^{-1}. Panel (d) sketches the structure of the biaxial smectic phase, corresponding to (a). Reproduced from Ref. [53•].

microparticles. For these two size ranges the details of the SAXS setups are distinctly different. The structure formed by *cubic nanoparticles* can be studies with conventional SAXS setups but also grazing incidence small- and wide-angle X-ray scattering (GISAXS and GIWAXS) can be employed [64••,65,68–71]. In contrast, for the larger *cubic microparticles* the use of a SAXS with a microradian resolution setup [7,20••] is imperative to visualise the Bragg peaks [66,67•]. Although similar packing constrains arise from the cubic shape of the *nanoparticles* and *microparticles*, their respective sizes and hence nature (single nanocrystal versus amorphous bulk material) influence the interactions between the particles as well as the self-assembly pathways that occur.

The focus of the first SAXS studies has been revealing the bulk crystal structure formed by the cubic particles. One of the main findings is that small structural changes in the exact cubic shape will change the final superlattice structure [64••,66,68,71]. For cubic nanoparticles made from palladium with a near perfect cubic shape Zhang et al. [64••] showed using SAXS that a simple cubic (SC) lattice will be formed in concentrated dispersions. In addition, they showed that by changing the ligand shell thickness a transition into a rhombohedral (RH) phase was induced. Fig. 6a shows the evolution of the obtained 2D SAXS patterns and corresponding structure factors S(q) from state C_{L1} to C_{L6} as the ligand shell increases. The C_{L1} state, indexed with a SC-lattice, can be recovered by dilution of the solvent as clearly seen in the S(q) peaks of state C_{L7} — that matches state C_{L1} again. Meijer et al. [66] subsequently showed with SAXS for cubic microparticles made from silica with intrinsic rounded corners that a hollow-site stacking structure very similar to a face centred cubic (FCC) lattice was obtained via convective assembly methods. A different modification of the cubic shape namely truncation of the cube corners will also change the crystal structure as shown by Disch et al. [68]. For slightly truncated cubic nanoparticles their GISAXS investigations showed that controlled self-assembly of the nanoparticles led to a highly ordered body-centred tetragonal (BCT) lattice. In a second GISAXS study by Disch et al. [71], it was shown that the structure formation is driven by the degree of truncation of the cube as assembly of cubic nanoparticles with a higher degree of truncation resulted in an FCC superlattice.

The SAXS investigations have also provided invaluable information on the cube assembly process in situ. The structural transition observed by Zhang et al. [64••] as described above, was actually performed in situ by slowly evaporating the solvent in which the cubic nanoparticles were suspended. This structural change could not have been visualised with other techniques. Similarly, Choi et al. [69] studied the assembly of cubic nanoparticles of lead selenite (PbSe) during evaporation of the solvent with GISAXS. They showed that by dynamic control over the solvent vapour environment they could follow the evolution of the superlattice structure from an initial FCC to a dried RH superlattice. In addition, the cubic nanoparticles were found to have two different orientations in the dispersion during assembly, namely flat at the sample container wall and tilted at the solvent–air interface. In another study, Meijer et al. [67•] investigated the in situ assembly of cubic silica microparticles with a magnetic core under the influence of gravity and an external magnetic field. The 2D SAXS patterns showed that at the continuously forming sediment fluid–solid interface these cubic microparticles formed a body centred monoclinic (BCM) lattice aligned to the magnetic field (Fig. 6b–d). Interestingly, these cubic microparticles were able to form a single crystal structure over the full sample volume illuminated with the X-ray beam, showing clear Bragg peaks with square symmetry (Fig. 6c) instead of the crystalline powder rings

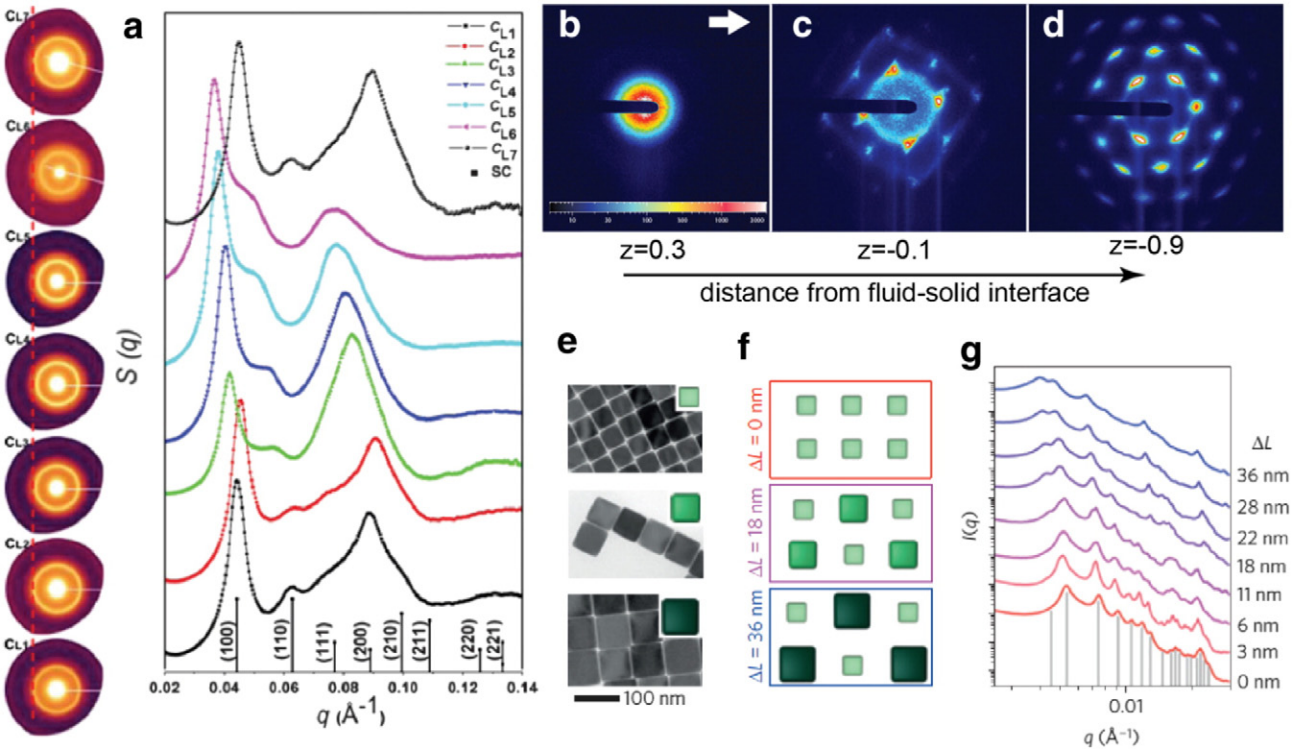

Fig. 6. a) Evolution of the 2D SAXS patterns and corresponding structure factors S(q) of assembled palladium nanocubes upon evaporation of ligand-rich solution which effectively rounds off the particle corners. The initial state C_{L1} is indexed with a SC lattice which slowly changes into an RH lattice for final state C_{L6}. Adapted from ref [64••] under license from APS. b–d) 2D SAXS patterns of the dispersion of cubic silica microparticles with a magnetic core in a 25 mT magnetic field after 12 h of sedimentation, taken around the fluid–solid interface, z = 0 mm, of the forming sediment where a BCM lattice forms. White arrow in b) indicates direction of B-field. A clear structural change is observed in the form of a transformation of square symmetry to hexagonal symmetry in the 2D SAXS pattern, caused by a rotation of the BCM lattice. Adapted from Ref. [67•] with permission from The Royal Society of Chemistry. e–f) Two collections of cube PAEs with complementary DNA but different edge lengths were co-crystallised to investigate the effect of size complementarity. e) Cube edge length was varied from 47 to 85 nm, as shown by TEM images, where each cube size has a variation in edge length < 5%. f) The difference in edge length (1 L) between these two collections was systematically varied from 0 nm (red, high size complementarity) to 38 nm (blue, low size complementarity). g) SAXS spectra plotted in a log–log format, with I(q) normalised by the intensity of the first peak. Ideal peak positions are given in grey for the ΔL = 0 sample. Crystal symmetry is maintained as ΔL increases, whereas peak breadth and peak position change. Adapted by permission from Macmillan Publishers Ltd: Nature Materials [65], copyright (2015).

typically observed for cubic nanoparticles (Fig. 6a). Moreover, the measurements showed that this structure rotated after time in the sediment indicated by hexagonal symmetry of the 2D SAXS pattern (Fig. 6d), which was attributed to an increased pressure resulting from the particles own weight and alignment with the capillary walls of the cubes flat faces.

In addition to structural and in situ analysis, the SAXS investigations can also probe the changes in crystal quality induced by particle size and shape polydispersity. A very recent study of O'Brien et al. [65] focussed on the effect of size and shape complementarity of cubic gold nanoparticles by using DNA as a surface ligand. They showed with SAXS that by increasing the size mismatch between the cubic nanoparticles resulted in a decrease in crystal domain size. While mixing particles with good complementary shapes, i.e. perfect cubes with perfect cubes or particles with convex faces with ones having concave faces, results in long-range ordered co-crystals. Fig. 6e–f shows TEM images of the different cubes that were used and schematic illustrations of the formed structures. The change in the radial averaged SAXS patterns and widening of the Bragg peaks, a direct result of decreasing domain size, is shown in Fig. 6g.

All the above mentioned studies illustrate the capabilities of using SAXS complementary to other techniques for the structural determination of ordered assemblies of anisotropic particles with unique complexity. A fascinating improvement that will allow more people to use SAXS for the investigation of the self-assembled structures of anisotropic particles, is the modelling and analysis of 1D SAXS data of periodic lattices of arbitrary nano-particles developed by Gang and co-workers [72•]. Hopefully, this or a similar method will also be extended to 2D SAXS analysis in the future for analysis of cubic microparticles.

6. Discussion & conclusion

The take-home message of this review is two-fold. Firstly, it formulates requirements for an 'ideal' SAXS beamline to study ordered colloidal systems of different type and with various degree of periodic order. It is shown that the challenging resolution problem can be solved using a microradian X-ray diffraction scheme. Secondly, it provides an overview of recent studies on particle shape effects in colloidal crystals and colloidal liquid crystals. This overview illustrates the strength of SAXS for investigations of periodic order in colloidal systems.

The colloidal scale ranges from a few nanometres to about a micron. To fully cover this scale of interest the 'ideal' SAXS beamline has to provide a minimum value of the scattering wavevector q_{min}, at which reliable data can still be measured, to be at least 2 times smaller than the position of the lowest-order diffraction peak. To work with micron-sized colloids one would therefore need $q_{min} \sim 3 \times 10^{-3}$ nm^{-1} or, in angular terms, $2\theta_{min} \sim 50$ μrad. Moreover, to fully describe periodic order extending over many lattice periods, one needs the actual resolution of the setup δq to be much better than the q_{min} value mentioned above. The setup described in this review yields a resolution $\delta(2\theta)$ down to a few microradians. Finally, another important parameter is the maximum value of the scattering wavevector, q_{max}, which defines the smallest scale available in the data. A broad q-range is important, for example, for liquid-crystalline phases of highly anisometric particles.

In the last decades the self-organisation of anisotropic colloidal particles has attracted significant attention in the search for new nanomaterials that can be prepared via the cheaper bottom-up approach. The particle shape variations are shown to be a key feature in tuning colloidal architectures. In this respect the SAXS investigations

reviewed here have shown to contribute significantly in resolving the crystal structures of anisotropic particles. These findings include the observations of nematic, smectic and columnar liquid crystals, as well as a very rare finding of the biaxial nematic phase, for rod-like, plate-like and board-like particles, respectively. In addition, we highlight the recent SAXS studies on the assembly of cube-like particles, which are promising candidates for high density close-packed structures.

On the basis of the considerations given above, the authors are of opinion that high resolution SAXS can be used more often in the research on colloidal particles and, especially, colloidal crystals and colloidal liquid crystals. The technique has a wide applicability to practically all colloidal systems and does not require drying, careful index matching and/or fluorescent labelling, which are needed for conventional microscopy techniques. With the increasing interest in the assembly of anisotropic particles, which are typically made from metal based materials, SAXS is the only technique that is suitable for in situ quantitative structural investigation. Furthermore, the structural investigations of fluorescent colloidal systems with radii of >400 nm that have been abundantly performed with confocal laser scanning microscopy can now be relatively easily extended with SAXS by employing the microradian resolution setup. However, to satisfy this request of the colloid community, more SAXS beamlines have to be (re)designed to provide sufficiently small $q_{\min}$ and, especially, δq to be suitable for studies of periodically-ordered colloidal systems. The authors hope that the current review will promote further collaboration between the colloid and SAXS communities.

Acknowledgements

The concepts of microradian X-ray diffraction were developed in close collaboration with Anatoly Snigirev (ESRF). The authors significantly profited from fruitful interactions with Henk Lekkerkerker and Albert Philipse (Utrecht University).

References[•,••]

[1] Narayanan T. High brilliance small-angle X-ray scattering applied to soft matter. Curr Opin Colloid Interface Sci 2009;14:409–15.
[2] Stribeck N. X-ray scattering of soft matter. Springer; 2007.
[3] O'Brien MG, Beale AM, Weckhuysen BM. The role of synchrotron radiation in examining the self-assembly of crystalline nanoporous framework materials: from zeolites and aluminophosphates to metal organic hybrids. Chem Soc Rev 2010;39:4767–82.
[4] Perez J, Nishino Y. Advances in X-ray scattering: from solution SAXS to achievements with coherent beams. Curr Opin Struct Biol 2012;22:670–8.
[5] Petoukhov MV, Svergun DI. Applications of small-angle X-ray scattering to biomacromolecular solutions. Int J Biochem Cell Biol 2013;45:429–37.
[6] Hell SW, Wichmann J. Breaking the diffraction resolution limit by stimulated-emission–stimulated-emission-depletion fluorescence microscopy. Opt Lett 1994;19:780–2.
[7] Thijssen JHJ, Petukhov AV, Hart DC't, Imhof A, van der Werf CHM, Schropp REI, et al. Characterization of photonic colloidal single crystals by microradian X-ray diffraction. Adv Mater 2006;18:1662–6.
[8] Pal A, Malik V, He L, Erne BH, Yin Y, Kegel WK, et al. Tuning the colloidal crystal structure of magnetic particles by external field. Angew Chem Int Ed 2015;54:1803–7.
[9] Glotzer SC, Solomon MJ. Anisotropy of building blocks and their assembly into complex structures. Nat Mater 2007;6:557–62.
[10] van Blaaderen A. Materials science — colloids get complex. Nature 2006;439:545–6.
[11] Damasceno PF, Engel M, Glotzer SC. Predictive self-assembly of polyhedra into complex structures. Science 2012;337:453–7.
[12] Guinier A. X-ray diffraction. Crystals, Imperfect Crystals and Amorphous Bodies. New York: Dover Publications; 1994.
[13] Sulyanova EA, Shabalin A, Zozulya AV, et al. Structural evolution of colloidal crystal films in the process of melting revealed by Bragg peak analysis. Langmuir 2015;31:5274–83.
[14] Hilhorst J, Abramova VV, Sinitskii A, et al. Double stacking faults in convectively assembled crystals of colloidal spheres. Langmuir 2009;25:10408–12.
[15] Meijer J, de Villeneuve VWA, Petukhov AV. In-plane stacking disorder in polydisperse hard sphere crystals. Langmuir 2007;23:3554–60.
[16] Yagi N, Inoue K. Ultra-small-angle X-ray diffraction and scattering experiments using medium-length beamlines at SPring-8. J Appl Crystallogr 2003;36:783–6.
[17] Als-Nielsen J, McMorrow D. Elements of modern X-ray physics. Wiley; 2011.
[18] ESRF upgrade programme phase II (2015–2022): technical design study. Grenoble, France: ESRF; 2015.
[19••] Snigirev A, Kohn V, Snigireva I, Lengeler B. A compound refractive lens for focusing high-energy X-rays. Nature 1996;384:49–51.
Introduction of x-ray refractive optics.
[20••] Petukhov AV, Thijssen JHJ, 't Hart DC, Imhof A, van Blaaderen A, Dolbnya IP, et al. Microradian X-ray diffraction in colloidal photonic crystals. J Appl Crystallogr 2006;39:137–44.
Principles of microradian diffraction.
[21] Borsboom M, Bras W, Cerjak I, et al. The Dutch-Belgian beamline at the ESRF. J Synchrotron Radiat 1998;5:518–20.
[22•] Petukhov AV, Aarts DGAL, Dolbnya IP, de Hoog EHA, Kassapidou K, Vroege GJ, et al. High-resolution small-angle x-ray diffraction study of long-range order in hard-sphere colloidal crystals. Phys Rev Lett 2002;88:208301.
Analysis of longitudinal coherence of an x-ray wave in small-angle diffraction.
[23] Petukhov AV, Dolbnya IP, Aarts DGAL, Vroege GJ. Destruction of long-range order recorded with in situ small-angle x-ray diffraction in drying colloidal crystals. Phys Rev E 2004;69:031405.
[24] Zocher H. Über freiwillige Strukturbildung in Solen. (Eine neue Art anisotrop flüssiger Medien.). Z Anorg Allg Chem 1925;147:91–110.
[25] Lekkerkerker HNW, Vroege GJ. Liquid crystal phase transitions in suspensions of mineral colloids: new life from old roots. Philos Trans R Soc A Math Phys Eng Sci 2013;371:20120263.
[26] Oldenbourg R, Wen X, Meyer RB, Caspar DLD. Orientational distribution function in nematic tobacco-mosaic-virus liquid-crystals measured by X-ray-diffraction. Phys Rev Lett 1988;61:1851–4.
[27] Li LS, Alivisatos AP. Semiconductor nanorod liquid crystals and their assembly on a substrate. Adv Mater 2003;15:408–11.
[28] Zhang ZX, van Duijneveldt JS. Isotropic-nematic phase transition of nonaqueous suspensions of natural clay rods. J Chem Phys 2006;124:154910.
[29] Dessombz A, Chiche D, Davidson P, Panine P, Chaneac C, Jolivet JP. Design of liquid-crystalline aqueous suspensions of rutile nanorods: evidence of anisotropic photocatalytic properties. J Am Chem Soc 2007;129:5904–9.
[30••] Kuijk A, Byelov DV, Petukhov AV, van Blaaderen A, Imhof A. Phase behavior of colloidal silica rods. Faraday Discuss 2012;159:181–99.
New model system of rods that can be studied by microradian SAXS as well as optical microscopy.
[31] Langmuir I. The role of attractive and repulsive forces in the formation of tactoids, thixotropic gels, protein crystals and coacervates. J Chem Phys 1938;6:873–96.
[32•] Brown ABD, Ferrero C, Narayanan T, Rennie AR. Phase separation and structure in a concentrated colloidal dispersion of uniform plates. Eur Phys J B 1999;11:481–9.
First observation of the columnar phase for plate-like colloids.
[33] Veerman JAC, Frenkel D. Phase-behavior of disk-like hard-core mesogens. Phys Rev A 1992;45:5632–48.
[34] Qazi SJS, Karlsson G, Rennie AR. Dispersions of plate-like colloidal particles — cubatic order? J Colloid Interface Sci 2010;348:80–4.
[35•] van der Kooij FM, Kassapidou K, Lekkerkerker HNW. Liquid crystal phase transitions in suspensions of polydisperse plate-like particles. Nature 2000;406:868–71.
First observation of the nematic/columnar LC phase transition for plate-like colloids.
[36•] Petukhov AV, van der Beek D, Dullens RPA, Dolbnya IP, Vroege GJ, Lekkerkerker HNW. Observation of a hexatic columnar liquid crystal of polydisperse colloidal disks. Phys Rev Lett 2005;95:077801.
Extensive analysis of the periodic order in a columnar LC colloid using high-resolution SAXS.
[37] Byelov DV, Mourad MCD, Snigireva I, Snigirev A, Petukhov AV, Lekkerkerker HNW. Experimental observation of fractionated crystallization in polydisperse platelike colloids. Langmuir 2010;26:6898–901.
[38] Mourad MCD, Byelov DV, Petukhov AV, de Winter DAM, Verkleij AJ, Lekkerkerker HNW. Sol–gel transitions and liquid crystal phase transitions in concentrated aqueous suspensions of colloidal gibbsite platelets. J Phys Chem B 2009;113:11604–13.
[39] Kleshchanok D, Holmqvist P, Meijer J, Lekkerkerker HNW. Lyotropic smectic B phase formed in suspensions of charged colloidal platelets. J Am Chem Soc 2012;134:5985–90.
[40] Gabriel JCP, Camerel F, Lemaire BJ, Desvaux H, Davidson P, Batail P. Swollen liquid-crystalline lamellar phase based on extended solid-like sheets. Nature 2001;413:504–8.
[41] Davidson P, Gabriel JCP. Mineral liquid crystals. Curr Opin Colloid Interface Sci 2005;9:377–83.
[42•] Miyamoto N, Nakato T. Liquid crystalline inorganic nanosheet colloids derived from layered materials. Isr J Chem 2012;52:881–94.
Extensive recent review of exfoliated inorganic nanosheets.
[43••] Michot LJ, Bihannic I, Maddi S, Funari SS, Baravian C, Levitz P, et al. Liquid-crystalline aqueous clay suspensions. Proc Natl Acad Sci U S A 2006;103:16101–4.
First reproducible observation of a nematic phase in platelike clay systems.
[44] Michot LJ, Paineau E, Bihannic I, Maddi S, Duval JFL, Baravian C, et al. Isotropic/nematic and sol/gel transitions in aqueous suspensions of size selected nontronite NAul. Clay Miner 2013;48:663–85.
[45] Davidson P. Vanadium pentoxide gels: from “chimie douce” to “matiere molle”. C R Chim 2010;13:142–53.

• of special interest.
•• of outstanding interest.

[46] Lemaire BJ, Davidson P, Ferre J, Jamet JP, Panine P, Dozov I, et al. Outstanding magnetic properties of nematic suspensions of goethite (alpha-FeOOH) nanorods. Phys Rev Lett 2002;88:125507.
[47••] Lemaire BJ, Davidson P, Ferre J, Jamet JP, Petermann D, Panine P, et al. The complex phase behaviour of suspensions of goethite (alpha-FeOOH) nanorods in a magnetic field. Faraday Discuss 2005;128:271–83.
Discussion of coupling of LC and magnetic behaviour of goethite nanorods.
[48] Lemaire BJ, Davidson P, Panine P, Jolivet JP. Magnetic-field-induced nematic-columnar phase transition in aqueous suspensions of goethite (alpha-FeOOH) nanorods. Phys Rev Lett 2004;93:267801.
[49] van den Pol E, Petukhov AV, Thies-Weesie DME, Vroege GJ. Simple rectangular columnar phase of goethite nanorods and its martensitic transition to the centered rectangular columnar phase. Langmuir 2010;26:1579–82.
[50•] Vroege GJ, Thies-Weesie DME, Petukhov AV, Lemaire BJ, Davidson P. Smectic liquid-crystalline order in suspensions of highly polydisperse goethite nanorods. Adv Mater 2006;18 [2565-+].
First observation of smectic LC in boardlike colloids.
[51] van den Pol E, Thies-Weesie DME, Petukhov AV, Vroege GJ, Kvashnina K. Influence of polydispersity on the phase behavior of colloidal goethite. J Chem Phys 2008;129:164715.
[52] Thies-Weesie DME, de Hoog JP, Mendiola MHH, Petukhov AV, Vroege GJ. Synthesis of goethite as a model colloid for mineral liquid crystals. Chem Mater 2007;19:5538–46.
[53•] van den Pol E, Petukhov AV, Thies-Weesie DME, Byelov DV, Vroege GJ. Experimental realization of biaxial liquid crystal phases in colloidal dispersions of boardlike particles. Phys Rev Lett 2009;103:258301.
First observation of a biaxial nematic LC in colloidal systems.
[54] van den Pol E, Thies-Weesie DME, Petukhov AV, Byelov DV, Vroege GJ. Uniaxial and biaxial liquid crystal phases in colloidal dispersions of board-like particles. Liq Cryst 2010;37:641–51.
[55] Luckhurst GR, Sluckin TJ. Biaxial nematic liquid crystals: theory, simulation and experiment. Chichester, UK: John Wiley & Sons Ltd; 2015.
[56] Vroege GJ. Biaxial phases in mineral liquid crystals. Liq Cryst 2014;41:342–52.
[57] Leferink Op Reinink ABGM, van den Pol E, Petukhov AV, Vroege GJ, Lekkerkerker HNW. Phase behaviour of lyotropic liquid crystals in external fields and confinement. Eur Phys J Spec Top 2013;222:3053–69.
[58] van der Beek D, Davidson P, Wensink HH, Vroege GJ, Lekkerkerker HNW. Influence of a magnetic field on the nematic phase of hard colloidal platelets. Phys Rev E 2008;77:031708.
[59] Abecassis B, Lerouge F, Bouquet F, Kachbi S, Monteil M, Davidson P. Aqueous suspensions of GdPO4 nanorods: a paramagnetic mineral liquid crystal. J Phys Chem B 2012;116:7590–5.
[60] van den Pol E, Lupascu A, Diaconeasa MA, Petukhov AV, Byelov DV, Vroege GJ. Onsager revisited: magnetic field induced nematic-nematic phase separation in dispersions of goethite nanorods. J Phys Chem Lett 2010;1:2174–8.
[61] van den Pol E, Petukhov AV, Byelov DV, Thies-Weesie DME, Snigirev A, Snigireva I, et al. Behavior of the smectic A phase of colloidal goethite in a magnetic field. Soft Matter 2010;6:4895–9.
[62] Leferink Op Reinink ABGM, Belli S, van Roij R, Dijkstra M, Petukhov AV, Vroege GJ. Tuning biaxiality of nematic phases of board-like colloids by an external magnetic field. Soft Matter 2014;10:446–56.
[63] Mertelj A, Lisjak D, Drofenik M, Copic M. Ferromagnetism in suspensions of magnetic platelets in liquid crystal. Nature 2013;504:237–41.
[64••] Zhang YG, Lu F, van der Lelie D, Gang O. Continuous phase transformation in nanocube assemblies. Phys Rev Lett 2011;107:135701.
First observation of phase transitions in cubic nanoparticle superlattices
[65] O'Brien MN, Jones MR, Lee B, Mirkin CA. Anisotropic nanoparticle complementarity in DNA-mediated co-crystallization. Nat Mater 2015;14:833–9.
[66] Meijer J, Hagemans F, Rossi L, Byelov DV, Castillo SIR, Snigirev A, et al. Self-assembly of colloidal cubes via vertical deposition. Langmuir 2012;28:7631–8.
[67••] Meijer J, Byelov DV, Rossi L, Snigirev A, Snigireva I, Philipse AP, et al. Self-assembly of colloidal hematite cubes: a microradian X-ray diffraction exploration of sedimentary crystals. Soft Matter 2013;9:10729–38.
Detailed study on the effect of shape and magnetic fields on cubic microparticle assembly.
[68] Disch S, Wetterskog E, Hermann RP, Salazar-Alvarez G, Busch P, Brueckel T, et al. Shape induced symmetry in self-assembled mesocrystals of iron oxide nanocubes. Nano Lett 2011;11:1651–6.
[69] Choi JJ, Bian K, Baumgardner WJ, Smilgies D, Hanrath T. Interface-induced nucleation, orientational alignment and symmetry transformations in nanocube superlattices. Nano Lett 2012;12:4791–8.
[70] Boneschanscher MP, Evers WH, Geuchies JJ, et al. Long-range orientation and atomic attachment of nanocrystals in 2D honeycomb superlattices. Science 2014;344:1377–80.
[71] Disch S, Wetterskog E, Hermann RP, et al. Structural diversity in iron oxide nanoparticle assemblies as directed by particle morphology and orientation. Nanoscale 2013;5:3969–75.
[72•] Yager KG, Zhang Y, Lu F, Gang O. Periodic lattices of arbitrary nano-objects: modeling and applications for self-assembled systems. J Appl Crystallogr 2014;47:118–29.
Presentation of detailed model for analysis of 1D SAXS patterns of anisotropic nanoparticle structures